J. Iron Steel Res. Int. (2019) 26:1376–1384
https://doi.org/10.1007/s42243-019-00256-4

ORIGINAL PAPER

Stretch bending defect control of L-section SUS301L stainless-steel components with variable contour curvatures

Zheng-wei Gu[1] · Lei Jia[1] · Xin Li[1] · Li-juan Zhu[1] · Hong Xu[1] · Ge Yu[1,2]

Received: 13 December 2018 / Revised: 22 February 2019 / Accepted: 1 March 2019 / Published online: 12 April 2019

Abstract
The stretch bending of L-section variable-curvature SUS301L stainless-steel roof bending beams for metro vehicles was numerically simulated. The causes of defects such as wrinkling, section distortion, and poor contour accuracy were analysed, and the corresponding control methods were proposed. The simulation results demonstrated that wrinkling in the small-arc segment could be eliminated by setting the die clearance and adjusting the elongation reasonably. Owing to the sidewall shrinkage of the profile in the process of stretch bending, the die groove depth was correspondingly reduced. Each section of the profile was effectively supported by the bottom of the die groove, and the section distortion could be controlled. Springback was the main reason for the poor contour accuracy, which could be compensated by modifying the die surface based on the springback value. Using the above defect control methods, forming experiments were performed on a new type of stretch bending die with variable die clearance and groove depth developed in this work. Finally, high-quality components were obtained, which verified the efficacy of the defect control methods.

Keywords Stretch bending · L-section · Variable contour curvature · Stainless-steel profile · Defect control

1 Introduction

As the economy is becoming globalized, urban traffic congestion and global warming are becoming increasingly serious problems. Rail transportation has become well known owing to its capacity to move large volumes of freight inexpensively, comparatively lower energy use and hence lower environmental impact compared with road transportation, and high speed [1–4]. Stainless-steel body-work has many advantages, such as being lightweight, being safe to use, exhibiting high corrosion resistance, and having a long service life. SUS301L stainless steel is widely used in the production and manufacturing of metro vehicles [5, 6]. The stretch bending process is one of the main forming methods of bending stainless-steel profiles. The profile is stretched and bent simultaneously during the forming process, and the tensile force produces a relatively uniform stress on the cross section, thereby reducing the springback and improving the contour accuracy [7]. Nevertheless, stretch bending is a complex process with many process parameters and die structural parameters that need to be controlled. Extruded aluminium profiles are mostly used in traditional stretch bending, which have good cross-sectional consistency and stable internal stress. The stress release during the forming process is relatively uniform, so that the formed component has a good stability, cross section is not easily distorted, springback is small, and stretch bending process is simple. However, for profiles formed by bending of sheets, particularly asymmetric section profiles formed by bending of stainless-steel sheets, if multi-curvature contours intersect on the component, then it can easily cause instability, wrinkling, and section distortion in the process of stretch bending owing to the accuracy limitation of the sheet bending. Furthermore, the higher ratio of the strength to the elastic modulus of SUS301L stainless steel may induce significant elastic recovery after unloading. Therefore, the stretch bending process is much more complex. All these significantly affect the quality of the products [8–10].

✉ Ge Yu
yugejlu18@163.com

[1] Department of Materials Science and Engineering, Jilin University, Changchun 130022, Jilin, China

[2] Roll Forging Research Institute, Jilin University, Changchun 130022, Jilin, China

In recent years, most researches on controlling the defects in the stretch bending process were performed by adjusting the process parameters. Liu et al. [11] analysed the stretch bending process for asymmetric hollow aluminium alloy profiles, and the golden ratio method was used to optimize the post-stretching elongation. Gu et al. [12] theoretically analysed the causes of the stretch bending defects in a Z-section stainless-steel profile and suggested relevant control methods. Nakajima et al. [13] developed a press bending technology for obtaining extruded square tubes with highly accurate cross sections. Liu et al. [14–16] established an analytical model for the collapsing deformation of a thin-walled rectangular tube and studied the effect of different dies on the cross-sectional distortion. They also studied the wall thickness distribution of the tube under multi-die constraints in the rotary draw bending process. Fu et al. [17] studied a one-step simulation for the bending process of an extruded rectangular aluminium tube. Chen and Gao [18] analysed the effect of the process parameters on the springback of T-section aluminium extrusions in the stretch bending process. Shen et al. [19] investigated the relationship between the stress components and cross-sectional distortion of thin-walled rectangular wave guide tubes in the rotary draw bending process. Zhu and Stelson [20] developed a simplified two-flange model and established a real-time closed-loop control algorithm for the stretch bending of rectangular aluminium tubes to predict the springback. Ouakdi et al. [21] studied the effect of the holding force, stretch height, and die radius on the springback of U-section aluminium alloy profiles in stretch bending tests. Liang et al. [22] proposed and implemented a new type of flexible multi-point 3D stretch bending process for a high-speed train manufacture demand.

Obviously, most of the previous researches focused on how to control the forming defects by adjusting the process parameters. However, for stainless-steel components with less thickness, particularly the L-section variable-curvature stainless-steel components described in this paper, there are many serious defects in the actual forming process which delay the production cycle of the vehicle. Through our research, it is found that it is difficult to control all the defects effectively and ensure the accuracy of the components only by adjusting the process parameters. Although a reasonable die structure design can effectively compensate for this deficiency, there are few studies on this method at present. Accordingly, this work combined two optimization methods: process parameter adjustment and die structure improvement. Based on the numerical simulation results, the causes of such issues for L-section stainless-steel components with variable curvatures during the stretch bending process were analysed and the forming process parameters were optimized. In addition, we improved the traditional stretch bending die having equal die clearance and groove depth and developed a new type of die with variable die clearance and groove depth. Finally, to verify the correctness of these control methods, forming experiments were performed on the new die, and high-quality stretch bending components were obtained.

2 Simulation model for stretch bending

2.1 Material properties

SUS301L-ST stainless steel is often used in roof bending beams of metro vehicles having high-strength requirement. To obtain the material performance parameters, uniaxial tensile tests were conducted. When prepared, three test specimens were cut out along the longitudinal direction of the profile, and the influence of different locations was neglected. The geometrical dimension is shown in Fig. 1a. It was assumed that the behaviour of the material was isotropic and linear in the elastic range. The von Mises yield criterion was chosen to describe the plastic behaviour. For the hardening stage, the isotropic hardening model was used, and the Krupkowsky law was used to describe the true stress-strain behaviour of the material:

$$\sigma = K \cdot (\varepsilon_0 + \varepsilon_p)^n, \tag{1}$$

where σ is the true stress; ε_0 is the initial plastic strain; ε_p is the plastic strain; K is the hardening coefficient; and n is the strain strengthening coefficient. The true stress–true strain curve acquired by the tensile tests is shown in Fig. 1b, and some specific material performance data are shown in Table 1.

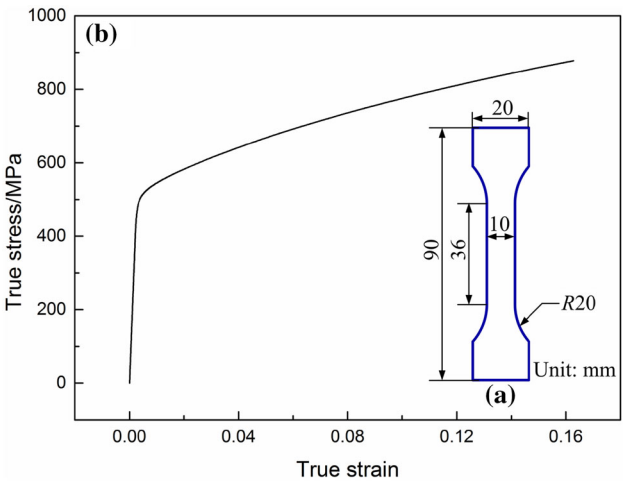

Fig. 1 Geometrical dimension of specimens for tensile tests (**a**) and true stress–true strain curve of SUS301L-ST stainless steel (**b**)

Table 1 Mechanical properties of SUS301L-ST stainless steel

Parameter	Value
Density/(kg m^{-3})	7850
Elastic modulus/GPa	191.04
Poisson's ratio	0.33
Yield strength/MPa	520.2
K/GPa	1.501
ε_0	0.0428
n	0.3365

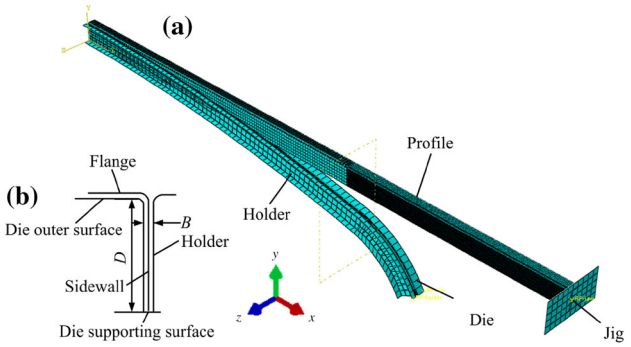

Fig. 3 Simulation model for stretch bending (**a**) and schematic of middle section of model (**b**)

2.2 Finite element model

The contour shape of the component contains two curves of different radii. The geometric shape and cross section of the component are shown in Fig. 2. ABAQUS was used to establish the finite element model, as shown in Fig. 3a. Owing to the symmetrical structure of the bending beam, only a half of the model needs to be analysed, which improves the computational efficiency. The model consists of a stretch bending die, jig, holder, and profile. The die and holder are fixed, and a symmetric constraint on the *x*-direction is applied to the profile, die, and holder. The jig is rigidly connected to the end of the profile, and the bending process is achieved by controlling the displacement of the jig. When the finite element analysis was performed, the profile was modelled as deformable shells with remaining parts modelled as discrete rigid bodies. The Coulomb friction model was selected to model the tangential contact behaviour, using a friction coefficient of 0.1. S4R element was used to discretize the profile. The size of the global element was 5 mm, but the fillet area and small-arc segment were defined using a 1-mm-element size. The rigid bodies were meshed using an R3D4 element with a global size of 10 mm, and the fillet areas of the die and holder were defined with a 1-mm-element size. For the stretch bending process, the dynamic explicit algorithm was used for double-precision calculation, significantly reducing the accumulation of the rounding errors and preventing the relative displacement of the grid nodes from causing deformation of the rigid body elements. Such a deformation on passing through the jig to the profile can lead to errors in the calculation results. The springback analysis used the implicit algorithm. Furthermore, the schematic of the middle section of the model is shown in Fig. 3b, where distance *B* between the die and holder is defined as the die clearance and distance *D* between the die outer surface and die supporting surface is the die groove depth.

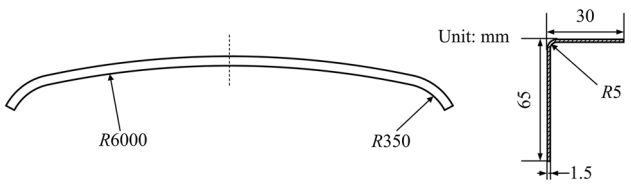

Fig. 2 Contour shape and cross section of L-section bending beam

2.3 Jig trajectory design

P–M–P loading mode was selected for the stretch bending. In this method, the pre-stretching force is first applied along the axial direction of the profile, and then, the profile is bent. Finally, after the bending, post-stretching is performed along the tangential direction of the section of the profile. In the stretch bending process, the jig is used to control the end of the profile, making it move and rotate to produce the desired bending, as shown in Fig. 4. This process is achieved in the finite element model by applying *x*-displacement and *y*-displacement loadings at the jig control point. It is assumed that the profile is completely attached to the die during the bending process, and the displacement of the control point in the *x* and *y* directions can be calculated for the component geometry. Referring to Fig. 5, we suppose that half of the profile length is *l*/2, radius of the large-arc segment on the die is *R*, angle at the centre is α, radius of the small-arc segment is *r*, and angle of the centre is β. The displacement coordinate functions of

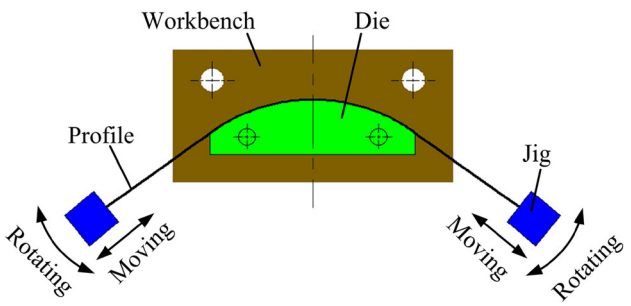

Fig. 4 Schematic of stretch bending equipment

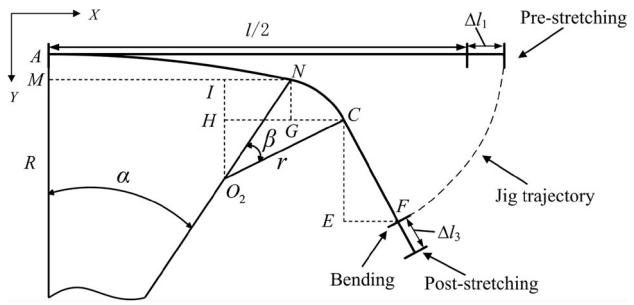

Fig. 5 Jig trajectory

the jig control point at the end of the current process are defined by $f(x)$ and $f(y)$, respectively.

Assuming that the pre-stretching elongation is Δl_1, then after the pre-stretching process, the following equation could be obtained.

$$f(x) = \frac{l}{2} + \Delta l_1 \tag{2}$$

$$f(y) = 0 \tag{3}$$

Then, the profile length after pre-stretching L could be:

$$L = \frac{l}{2} + \Delta l_1 \tag{4}$$

Assuming that the bending elongation is Δl_2, then after the bending process, $f(x)$ and $f(y)$ could be changed into:

$$\begin{aligned} f(x) &= MN + GC + EF = \\ &R\sin\alpha + HC - HG + CF\cos(\alpha+\beta) = \\ &R\sin\alpha + r\sin(\alpha+\beta) - r\sin\alpha + \\ &(L + \Delta l_2 - R\alpha - r\beta)\cos(\alpha+\beta) \end{aligned} \tag{5}$$

$$\begin{aligned} f(y) &= AM + IH + CE = \\ &R(1-\cos\alpha) + IO_2 - HO_2 + CF\sin(\alpha+\beta) = \\ &R(1-\cos\alpha) + r[\cos\alpha - \cos(\alpha+\beta)] + \\ &(L + \Delta l_2 - R\alpha - r\beta)\sin(\alpha+\beta) \end{aligned} \tag{6}$$

Finally, assuming that the post-stretching elongation is Δl_3, $f(x)$ and $f(y)$ were shown in the following equations after post-stretching process.

$$\begin{aligned} f(x) = R\sin\alpha + r\sin(\alpha+\beta) - r\sin\alpha + (L + \Delta l_2 - R\alpha - \\ r\beta + \Delta l_3)\cos(\alpha+\beta) \end{aligned} \tag{7}$$

$$\begin{aligned} f(y) = R(1-\cos\alpha) + r[\cos\alpha - \cos(\alpha+\beta)] + (L + \Delta l_2 - \\ R\alpha - r\beta + \Delta l_3)\sin(\alpha+\beta) \end{aligned} \tag{8}$$

As l, R, r, α, and β are known, given Δl_1, Δl_2, and Δl_3, the coordinates of the jig in the three processes can be determined by Eqs. (2)–(8). In ABAQUS, the movement through the calculated trajectory is controlled by altering the jig displacement amplitude.

3 Simulation results and discussion

3.1 Analysis of forming defects

In this work, elongation is defined as the total stretching length in the stretch bending process, i.e. elongation is the sum of the pre-stretching elongation, bending elongation, and post-stretching elongation. At first, the elongation is selected as 5% of the initial profile length. The die is designed to have equal die clearance, and its size is 1.5 times the profile thickness. Simultaneously, it has a constant groove depth, equal to the difference between the height of the sidewall and the profile thickness, so that the initial groove depth is 63.5 mm. Some of the main forming defects produced after the end of the stretch bending are shown in Fig. 6. It can be seen that the main defects of the component are sidewall wrinkling, section distortion, and poor contour accuracy.

As shown in Fig. 6b, when the die clearance is set as 1.5 times the profile thickness, there is obvious wrinkling in the sidewall of the small-arc segment with a radius of 350 mm. This is due to the thinner wall thickness of the component, long sidewall height, small bending radius, and large bending angle. Buckling occurs when the tangential stress on the inner layer of the sidewall reaches a critical value during the stretch bending. Stretch bending exerts tension on the profile so that the neutral layer moves down and eventually moves out of the profile, so that all the sections of the profile experience tensile stress. However, in this work, the studied profile has a high sidewall and so requires a large elongation to completely remove the stress neutral layer in the profile, which will lead to drastic thinning and section distortion. Therefore, wrinkling cannot be solved only by stretching. Die clearance can affect the contact stress between the profiles and dies, thereby affecting the stress distribution of the profiles in the process of stretch bending, which has a significant impact on wrinkling. Therefore, the effect of the die clearance and elongation on wrinkling is studied in this work. Maximum normal height difference ΔH between adjacent wrinkled peaks and troughs of the bottom edge of the neutral layer of the profile sidewall is used to represent the degree of wrinkling.

In the process of plastic deformation, according to the rule of volume invariance, as the elongation increases during the stretch bending process, the profile elongates along the axial direction and the section shrinks gradually. With continuous stretching, the shortening of the sidewall gradually makes it difficult to obtain the support of the bottom of the die groove. When a bending force is applied, fillet collapsing occurs owing to the lack of effective support at the bottom of the profile, particularly in the small-

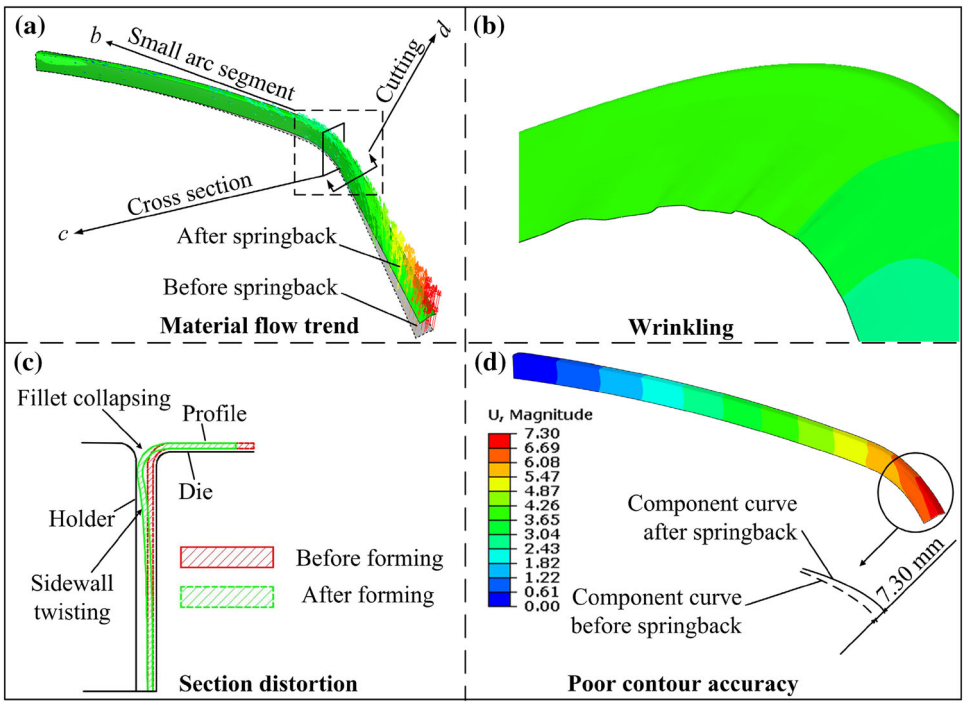

Fig. 6 Material flow trend of formed component during unloading process (**a**) and main defects of formed component after unloading process: wrinkling (**b**), section distortion (**c**), and poor contour accuracy (**d**)

arc segment, which simultaneously results in the sidewall twisting, as shown in Fig. 6c. The extent of the fillet collapsing represented by Z-direction displacement ΔC of the node at tangent is used to evaluate the degree of section distortion in the analysis.

According to the law of elastic–plastic coexistence, plastic deformation is maintained and elastic deformation is recovered after unloading. Therefore, springback is inevitable in the stretch bending process, which drastically affects the contour accuracy of the components. Figure 6a shows the material flow trend of the formed component with an addendum segment which has a large elastic recovery during the unloading process. After the forming is completed, the addendum segment is cut off to obtain the desired bending beam. Figure 6d shows the displacement nephogram of the bending beam after unloading. In this work, the maximum gap between the shape after the springback and shape of the target at the end of the bending beam after unloading is defined as the contour accuracy deviation, which is denoted by ΔS. The maximum contour accuracy deviation is 7.3 mm, which highly exceeds the accuracy requirement.

3.2 Sidewall wrinkling control

Die clearance and elongation are two important parameters affecting wrinkling. In the process of stretch bending, when the assembly difficulty between the die and profile is not significantly increased, the die clearance is generally minimally set, which will evidently affect the wrinkling trend. As shown in Fig. 7a, wrinkle height ΔH decreases with the decrease in the die clearance. However, wrinkling still exists. If the die clearance is extremely small, the assembly of the profile will be difficult because of the excessive friction between the profile and die. Therefore, reducing the die clearance cannot fundamentally eliminate the wrinkling. Elongation is also an important parameter that significantly affects wrinkling. When the die clearance is 1.1 times the profile thickness, the results under different elongations are shown in Fig. 7b. With the increase in the elongation, the wrinkling tendency of the formed component decreases gradually. When the elongation is 10% of the initial profile length, the wrinkling is basically eliminated. The reason is that full plastic deformation can compensate for wrinkling. Therefore, wrinkling can be eliminated by setting the die clearance and adjusting the elongation reasonably. For the component studied in this work, when the die clearance is 1.1 times the profile thickness and elongation is 10% of the initial profile length, wrinkling in the small-arc segment is basically eliminated.

3.3 Section distortion control

From the above analyses, it is known that the sidewall shrinkage of the profile during the stretch bending process is the main cause of the section distortion. Therefore, in

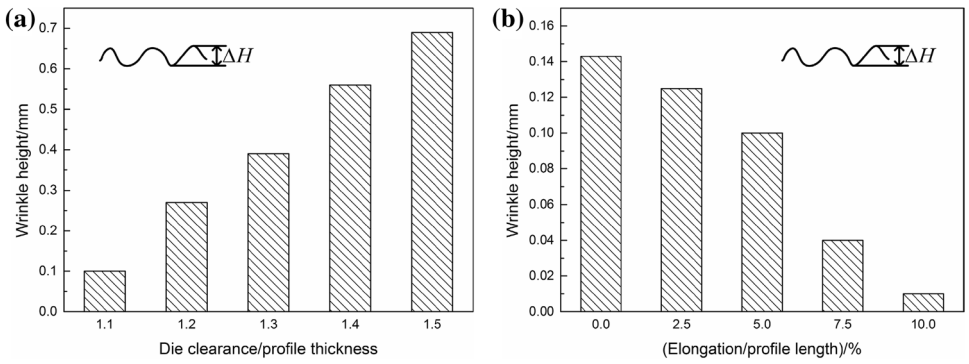

Fig. 7 Effect of die clearance (**a**) and elongation (**b**) on wrinkling

this work, the sidewall shrinkage of profiles can be compensated by setting the die groove depth reasonably. The result is that the profiles can be invariably and strongly supported by the die, and then, the section distortion during the stretch bending can be controlled. To obtain the sidewall shrinkage of each section after the stretch bending, the die groove is divided into eight sections S_1–S_8, and the nth section is defined as S_n as shown in Fig. 8a. In addition, d_n and d_n' are, respectively, defined as the heights of the sidewalls corresponding to the section of the nth die groove before and after the forming, i.e. the distance from the upper surface of the flange to the bottom of the sidewall. The height of the sidewall is uniform before forming, d_n= 65 mm. A_n is the sidewall shrinkage at the section of the nth die groove, so $A_n = d_n - d_n'$. D_{mn} is defined as the groove depth corresponding to the d_n' section when calculating the $(m + n)$th compensation. B_m is the sidewall shrinkage compensation coefficient, which represents the multiple of the sidewall shrinkage value. In this work, m = 0, 1, 2, 3, 4, 5, 6, and B_1 = 1.0, B_2 = 1.1, B_3 = 1.2, B_4 = 1.3, B_5 = 1.4, and B_6 = 1.5. When $m = 0$, D_{0n}= 63.5 mm and B_0 = 0, i.e. uniform groove depth, the groove is not modified. When $m \neq 0$, $D_{mn} = D_{0n} - B_m \times A_n$, i.e. based on the sidewall shrinkage of each section, die groove depth D_{mn} is corrected. Figure 8a shows the fillet collapse values of S_7 in the middle section of the small-arc segment under different sidewall shrinkage compensation coefficients when the elongation is 10% of the initial profile length. A negative value indicates fillet collapsing, whereas a positive value indicates fillet upwarping. The corresponding section deformations are shown in Fig. 8b. As can be seen from points a and b in Fig. 8, the section distortion decreases significantly with the increase in the sidewall shrinkage compensation coefficient. When the compensation coefficient is 1.1, the section deformation of the stretch bending component is small, and the cross section is basically undistorted, as shown at point c in Fig. 8. However, when the compensation coefficient is extremely large, fillet upwarping occurs owing to the small groove depth, as shown at point d in Fig. 8. Therefore, according to the sidewall shrinkage at the corresponding position, the groove depth at each section is reasonably set to effectively support the bottom of the sidewall in the process of stretch bending, thus controlling the section distortion. For the components studied in this work, when the elongation is 10% of the initial profile length, the appropriate die groove depth modified value is 1.1 times the profile sidewall shrinkage value.

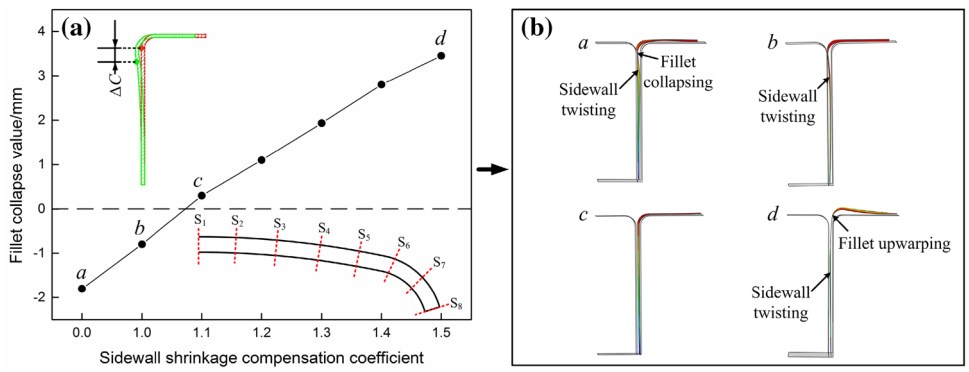

Fig. 8 Fillet collapse values (**a**) and section deformations (**b**) of S_7 for different sidewall shrinkage compensation coefficients

3.4 Contour accuracy control

The contour accuracy is poor because of a large springback. In this work, the contour accuracy of the stretch bending components was controlled by modifying the die surface. The die surface modification method utilizes the calculated springback value to compensate the die surface in the opposite direction, so that the formed component can meet the requirement of contour accuracy. The concrete implementation principle is to subtract the calculated springback value or its multiple from the coordinates of the die surface nodes to obtain a new die surface after the springback compensation. The newly obtained die surface is used to simulate the stretch bending again. A numerical simulation was used to yield the results, as shown in Fig. 9. It can be seen that based on the springback value, the contour accuracy can be effectively controlled by the die surface modification. When the elongation is 10% of the initial profile length and die surface modified value is 1.2 times the springback value, the contour accuracy of the stretch bending components is optimal and within the accuracy requirement of 1 mm. Therefore, it is suggested that the die surface modification method should be used to control the contour accuracy. For this work, when the elongation is 10% of the initial profile length, the appropriate die surface modified value is 1.2 times the springback value.

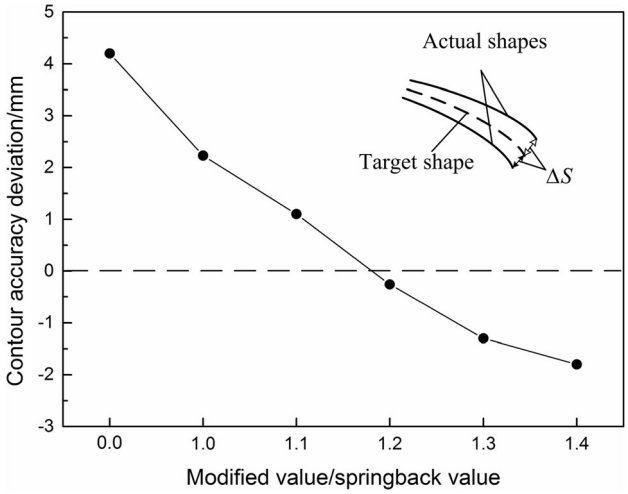

Fig. 9 Effect of die surface modified value on contour accuracy

4 Stretch bending experiments

The original stretch bending component before the defect control is shown in Fig. 10. The contour shape and cross-sectional features of the component make it prone to wrinkling (Fig. 10a) and section distortion (Fig. 10b) in the small-arc segment during the bending process. The section distortion includes the fillet collapsing and sidewall twisting (Fig. 10c). Moreover, for railway vehicle structural components, because of the large size characteristics, the springback is significant and the contour accuracy is difficult to control, as displayed in Fig. 10a. These defects strongly affect the forming precision of the stretch bending components, and the subsequent adjustment of the formed components is difficult, which leads to a poor assembly accuracy with other components.

Consequently, to obtain high-quality components, according to the above analyses, the die clearance of the small-arc segment should be set as 1.1 times the profile thickness, elongation should be 10% of the initial profile length, die groove depth modified value should be 1.1 times the sidewall shrinkage value, and die surface modified value should be 1.2 times the springback value. However, if the die is designed to have a uniform clearance, which is 1.1 times the profile thickness, the initial assembly of the profile is difficult because of the large

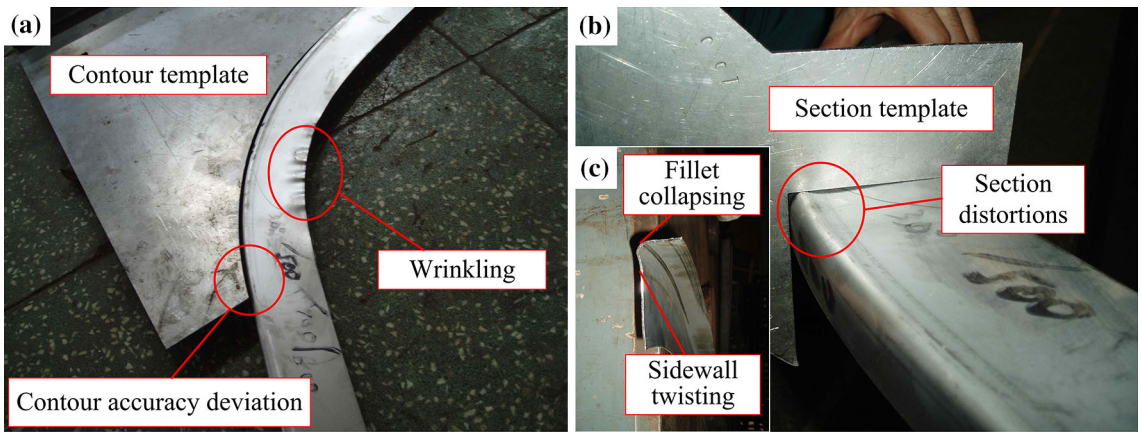

Fig. 10 Stretch bending component with wrinkling, poor contour accuracy (**a**), section distortion (**b**), and two forms of section distortion (**c**)

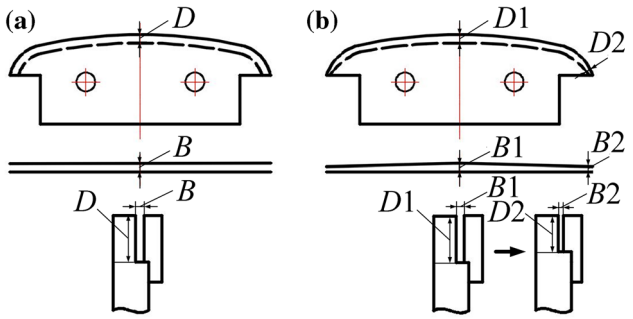

Fig. 11 Traditional stretch bending die (**a**) and new stretch bending die with variable die clearance and groove depth (**b**)

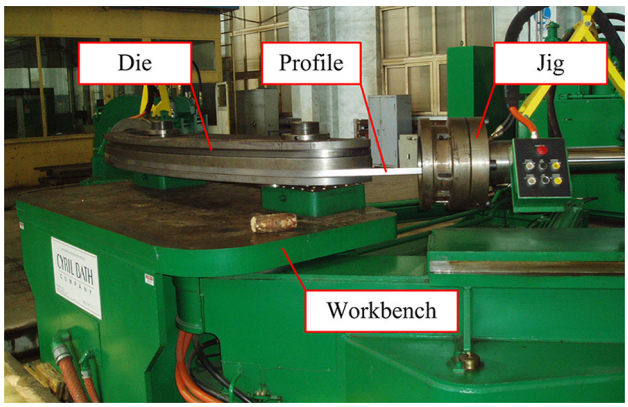

Fig. 12 Stretch bending experiment

friction between the profile and die. Therefore, the traditional stretch bending die (Fig. 11a) having uniform die clearance and uniform groove depth is improved and a new type of die (Fig. 11b) with variable die clearance and groove depth is developed. The die clearance gradually varies from the centre to the small-arc segment at both ends from 1.5 times ($B1$) to 1.1 times ($B2$) the profile thickness, so that the profile can be smoothly assembled and the small-arc segment can be effectively prevented from wrinkling. Simultaneously, according to the modified value of the die groove depth calculated by the simulation, the die groove depth also gradually varies from the centre of the die to the small-arc segment at both ends from $D1$ to $D2$.

To verify the validity of the research conclusion and rationality of the new die design, a die with variable die clearance and groove depth was processed. The forming experiments were conducted on an NC stretch bending machine imported from Cyril Bath Company in the USA, as shown in Fig. 12. After the experiments, high-quality stretch bending components were obtained. As shown in Fig. 13a, the sidewall is smooth and there is no wrinkling in the small-arc segment of the stretch bending component. Eight positions are selected in the S_7 section of the small-arc segment. A feeler gauge is applied to measure the gap between the section and square gauge (Fig. 13b), and the measurement results are defined as the section accuracy deviation, as shown in Fig. 14a. All the section accuracy deviations meet the accuracy requirement of less than 0.5 mm. As can be seen from Fig. 13c, the overall contour well fits the contour accuracy measurement template. The contour template was processed using a laser cutting method according to the outer surface curve of the standard component. Similarly, a feeler gauge was applied to measure the gap between the formed component and contour template. Eventually, the measurement results of the contour accuracy deviations are shown in Fig. 14b, which meet the requirement of the contour accuracy deviation being within 1 mm. The experimental results are basically in agreement with the finite element analyses. All these prove the effectiveness of the defect control measures described in this paper.

5 Conclusions

1. Based on the numerical simulation analysis of the stretch bending process, a new type of stretch bending die with variable die clearance and groove depth is developed. It resolves the issues caused by some stretch bending defects which cannot be solved by the

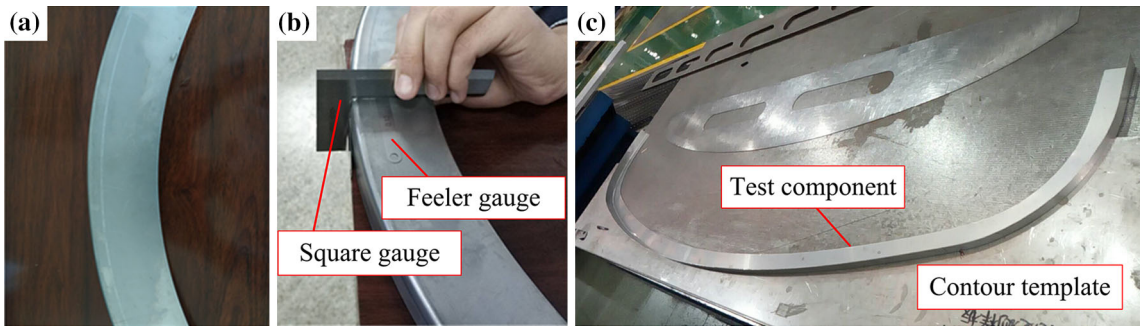

Fig. 13 High-quality stretch bending component without wrinkling (**a**) and section distortion (**b**), and with high contour accuracy (**c**)

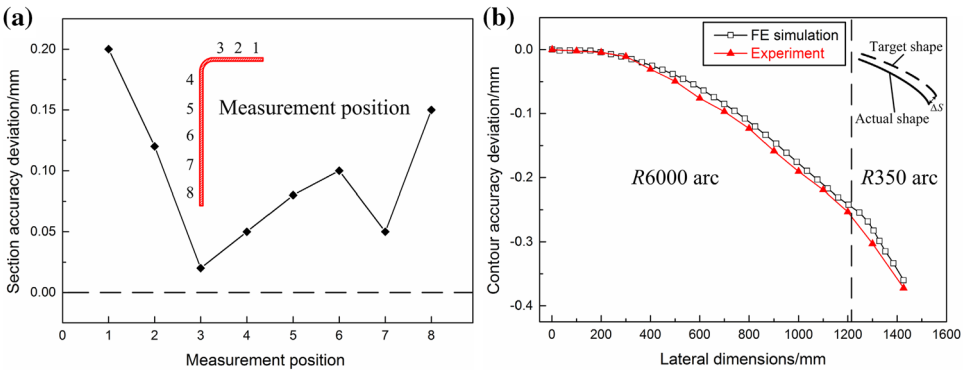

Fig. 14 Section accuracy deviation (**a**) and contour accuracy deviation (**b**) of component

traditional stretch bending die having uniform die clearance and groove depth.

2. The die clearance and elongation are the main process parameters affecting the wrinkling. For the components studied in this work, wrinkling in the small-arc segment is basically eliminated when the die clearance is 1.1 times the profile thickness and elongation is 10% of the initial profile length.
3. The section distortion in the L-section stretch bending component is mainly caused by sidewall shrinkage. They can be effectively eliminated by controlling the die groove depth to compensate for the sidewall shrinkage during the stretch bending. The appropriate die groove depth modified value is 1.1 times the sidewall shrinkage value.
4. The contour accuracy is poor owing to the significant springback. It can be effectively controlled by die surface modification based on the springback value. For the components studied in this work, a reasonable die surface modified value is 1.2 times the springback value.

Acknowledgements This work was financially supported by the National Natural Science Foundation of China (51101072) and Technology Development Program of Jilin Province (20150307015GX and 20160204058GX).

References

[1] M.V. Venkatesan, N. Murugan, B.M. Prasad, A. Manickavasagam, J. Iron Steel Res. Int. 20 (2013) No. 1, 71–78.
[2] K.Y. Wang, P.F. Liu, W.M. Zhai, C. Huang, Z.G. Chen, J.M. Gao, Sci. China (Technol. Sci.) 58 (2015) 226–235.
[3] L. Ling, X.B. Xiao, X.S. Jin, Acta Mech. Sin. 30 (2014) 860–875.
[4] K.W. Zhao, J.H. Zeng, X.H. Wang, J. Iron Steel Res. Int. 16 (2009) No. 3, 20–26.
[5] T. Tomioka, S. Tachikawa, Y. Akiyama, Mech. Eng. J. 4 (2017) 16–00467.
[6] M. Eskandari, A. Najafizadeh, A. Kermanpur, M. Karimi, Mater. Des. 30 (2009) 3869–3872.
[7] J. Zhao, R.X. Zhai, Z.P. Qian, R. Ma, Int. J. Mech. Sci. 75 (2013) No. 1, 45–54.
[8] F. Paulsen, T. Welo, J. Mater. Process. Technol. 58 (1996) 274–285.
[9] A.H. Clausen, O.S. Hopperstad, M. Laugseth, Int. J. Mech. Sci. 43 (2001) 427–453.
[10] O.S. Hopperstad, T. Berstad, H. Ilstad, O.G. Lademo, M. Langseth, J. Mater. Process. Technol. 80–81 (1988) 551–555.
[11] C.G. Liu, X.G. Zhang, X.T. Wu, Int. J. Adv. Manuf. Technol. 82 (2016) 1737–1746.
[12] Z.W. Gu, M.M. Lü, X. Li, H. Xu, J. Iron Steel Res. Int. 23 (2016) 525–530.
[13] K. Nakajima, N. Utsumi, M. Yoshida, Int. J. Precis. Eng. Manuf. 14 (2013) 965–970.
[14] K.X. Liu, Y.L. Liu, H. Yang, Int. J. Adv. Manuf. Technol. 69 (2013) 627–636.
[15] K.X. Liu, Y.L. Liu, H. Yang, Int. J. Precis. Eng. Manuf. 15 (2013) 633–641.
[16] K.X. Liu, Y.L. Liu, H. Yang, Int. J. Adv. Manuf. Technol. 68 (2013) 1867–1874.
[17] L.J. Fu, X.H. Dong, P. Wang, Int. J. Adv. Manuf. Technol. 43 (2009) 1069–1080.
[18] M.H. Chen, L. Gao, in: Z.J. Yuan, X.P. Xu (Eds.), Advances in Machining & Manufacturing Technology VIII, Key Engineering Materials, Hangzhou, 2006, pp. 416–420.
[19] H.W. Shen, Y.L. Liu, H.Y. Qi, H. Yang, S.H. Zhou, Int. J. Adv. Manuf. Technol. 68 (2013) 651–662.
[20] H. Zhu, K.A. Stelson, J. Manuf. Sci. Eng. 125 (2003) 113–119.
[21] E.H. Ouakdi, R. Louahdi, D. Khirani, L. Tabourot, Mater. Des. 35 (2012) 106–112.
[22] J.C. Liang, S. Gao, F. Teng, P.Z. Yu, X.J. Song, Int. J. Adv. Manuf. Technol. 71 (2014) 1939–1947.